Modeling Electrochemical Deposition inside Nanotubes to Obtain Metal−Semiconductor Multiscale Nanocables or Conical Nanopores

Konstantin Lebedev,[†,‡] Salvador Mafé,[†] and Pieter Stroeve*[,§]

Department de Termodinàmica, Universitat de València, E-46100 Burjassot, Spain, and Department of Chemical Engineering and Materials Science, University of California Davis, Davis, California 95616

Received: March 4, 2005; In Final Form: June 7, 2005

Nanocables with a radial metal−semiconductor heterostructure have recently been prepared by electrochemical deposition inside metal nanotubes. First, a bare nanoporous polycarbonate track-etched membrane is coated uniformly with a metal film by electroless deposition. The film forms a working electrode for further deposition of a semiconductor layer that grows radially inside the nanopore when the deposition rate is slow. We propose a new physical model for the nanocable synthesis and study the effects of the deposited species concentration, potential-dependent reaction rate, and nanopore dimensions on the electrochemical deposition. The problem involves both axial diffusion through the nanopore and radial transport to the nanopore surface, with a surface reaction rate that depends on the axial position and the time. This is so because the radial potential drop across the deposited semiconductor layer changes with the layer thickness through the nanopore. Since axially uniform nanocables are needed for most applications, we consider the relative role of reaction and axial diffusion rates on the deposition process. However, in those cases where partial, empty-core deposition should be desirable (e.g., for producing conical nanopores to be used in single nanoparticle detection), we give conditions where asymmetric geometries can be experimentally realized.

1. Introduction

Nanocables with radial heterostructures are of potential interest for electronics and biosensor applications. In particular, nanocables with a radial metal−semiconductor heterostructure have recently been prepared by electrochemical deposition inside metal nanotubes.[1] First, a bare nanoporous polycarbonate track-etched membrane is coated uniformly with a metal film by electroless deposition. The film forms a working electrode for further deposition of a semiconductor layer that grows radially inside the nanopore when the deposition rate is slow.[1] This is an important problem of mass transfer and chemical reaction for a multiscale nanomaterial; that is, one dimension is on the nanoscale, while another dimension is on the microscale. We propose a new physical model for the nanocable synthesis and study the effects of the deposited species concentration, potential-dependent reaction rate, and nanopore dimensions on the electrochemical deposition. Since axially uniform nanocables are needed for most applications, we consider the relative role of reaction and axial diffusion rates on the deposition process. However, in those cases where partial, empty-core deposition should be desirable (e.g., for producing conical nanopores to be used in single nanoparticle detection[2]), we give conditions where other geometries can be experimentally realized.

Electrochemical deposition is a subject of current scientific and technological importance, though most existing models tend to concentrate on the case of metal electrodeposition on electrodes, as shown in two recent examples.[3,4] During the last years, modeling of the electrochemical synthesis of metallic nanowires within porous membranes has also attracted attention because of its potential for nanotechnological applications. In particular, using a membrane as a template constitutes an alternative to traditional lithographic methods (see, e.g., ref 5 and references therein). However, the present problem requires considering simultaneously axial diffusion through the nanopore and radial transport to the nanopore surface, with a surface reaction rate that depends on both the axial position and time. This is so because the radial potential drop across the deposited semiconductor layer changes with the layer thickness through the nanopore. Although some reference will be made to the particular experimental situation of ref 1 where the reaction proceeded slowly (uniform deposition took 14 h), the model equations are general enough to be applied to other experimental regimes and transport problems in nanopores, such as electroless metal deposition.

2. Theoretical Model

Figure 1a shows a scheme of the nanocable that can result from electrochemical deposition of a semiconductor inside a metal nanotube. The membrane pore is first coated with a metal (Au in ref 1) film. Further deposition of a semiconductor (Te in ref 1) layer that grows radially inside the nanotube can produce a radially layered, metal−semiconductor heterostructure (nanocable). In the figure, L and R are the nanopore thickness and radius before the deposition and $R_s(x;t) \leq R$ is the effective, axial-dependent radius at time t (deposition starts at $t = 0$). Before presenting the equations characteristic of the deposition process, we must estimate the electric potential drop through the semiconductor layer because the reaction rate depends on the difference between the surface potential and the solution potential (see Figure 1a).

* Corresponding author. E-mail: pstroeve@ucdavis.edu.
[†] Universitat de València.
[‡] On leave from Department of Applied Mathematics, Kuban State University, 350040 Krasnodar, Russia.
[§] University of California Davis.

10.1021/jp051133f CCC: $30.25
Published on Web 07/13/2005

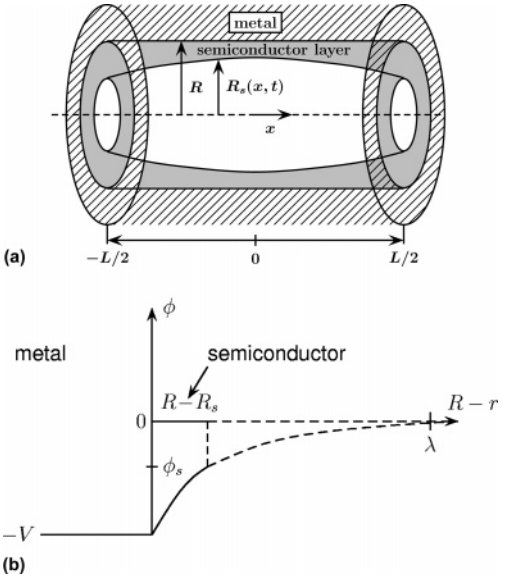

Figure 1. (a) Schematic view of the nanocable. The membrane pore is coated with a metal film. Further deposition of a semiconductor produces a radial metal−semiconductor heterostructure. L and R are the nanopore thickness and initial radius. $R_s(x;t)$ is the effective, axial-dependent radius at time t. The solution layer is located in the central region $0 \le r < R_s(x;t)$. (b) The ideal metal−semiconductor junction. The electric potential profile ϕ over $0 \le R - R_s(x;t) \le \lambda$ is obtained with the full depletion approximation.

Ideal Metal−Semiconductor Junction. The formation of a semiconductor layer by electrodeposition on a metallic surface is a complex process (see, e.g., refs 6−8 for Te deposited on Au surfaces in the presence of Cd, which is the case relevant to the experiments in ref 1). Moreover, real metal−semiconductor junctions are difficult to model because the physical realization of the junction leads to crystal structure defects and finite size effects.[9] Since we wish to concentrate our analysis on the effects of diffusion and surface kinetics on the electrodeposition occurring in the nanopore, we must introduce simplified models for the junction.

Figure 1b shows the scheme of an ideal metal−semiconductor junction for the case of an n-type semiconductor. The semiconductor layer is in the region $R_s(x;t) \le r \le R$, where r is the radial coordinate, and all of the potential drop occurs in the semiconductor because of the much smaller number of charge carriers (compared to the metal) there.[9,10] The electric potential profile in a semi-infinite semiconductor layer can be obtained by using the full depletion approximation. If we assume that the potential profile for the case of the actual semiconductor region in Figure 1a does not deviate significantly from the latter, we must solve the one-dimensional Poisson equation in the depleted layer model:[11]

$$\frac{d^2\phi}{d(R-r)^2} = \begin{cases} -\dfrac{FN_d}{\epsilon_s\epsilon_0}, & 0 < (R-r) < \lambda \\ 0, & (R-r) > \lambda \end{cases} \quad (1)$$

where the potential ϕ is in R_gT/F units, with R_g being the gas constant, T, the temperature, and F, the Faraday constant. In eq 1, λ is the depleted layer thickness, with ϵ_s and ϵ_0 being the semiconductor dielectric constant and the vacuum electrical permittivity, respectively, and N_d being the donor molar concentration.

Solution of eq 1 with the boundary conditions $\phi(0) = -V$ (the potential difference between the metal and the solution) and $\phi(\lambda) = 0$ gives the electric potential at the semiconductor surface $r = R_s(x;t)$ (see Figure 1b):

$$\phi_s(x;t) = -V\left[\frac{R - R_s(x;t)}{\lambda} - 1\right]^2 \quad (2)$$

Note that this potential changes with the axial position x through the nanopore (see Figure 1a). From eqs 1 and 2,

$$\lambda = \left(\frac{2\epsilon_s\epsilon_0 V}{FN_d}\right)^{1/2} \quad (3)$$

Substituting the typical values[1,11] $R \approx 10^{-8}$ m $< \lambda \approx 10^{-7}$ m in eq 2, we find that the surface potential in the reaction rate should be close to V, as shown schematically in Figure 1b.

Since the depleted layer thickness can be of the order of 100 nm, it is likely that interfacial effects rather than bulk behavior dictate the electric current in the deposited layer, which is proportional to the semiconductor deposition rate. Therefore, it would be questionable to assume bulk, ohmic behavior for the deposited layer, and the above analysis becomes necessary. Note that we have ignored the electrical double layer[12] in the solution close to the surface, which could be justified for high ionic strengths. This approximation, together with the highly idealized model used for the junction, makes it difficult to estimate the total potential difference between the semiconductor and the solution exactly. Therefore, the values for ϕ_s introduced here constitute only approximate estimations intended to show the effect of this parameter on the transport equations.

Transport Equations. We assume that the migrational transport can be neglected due to the high concentration of added electrolyte. The diffusion equation[13,14] for the transport through a nanopore is

$$\frac{\partial c(x,r;t)}{\partial t} = D\left[\frac{\partial^2 c(x,r;t)}{\partial x^2} + \frac{1}{r}\frac{\partial}{\partial r}\left(r\frac{\partial c(x,r;t)}{\partial r}\right)\right] \quad (4)$$

Since $R \approx 10$ nm $\ll 10$ μm $\approx L$, radial diffusion is very fast compared to axial diffusion and the concentration $c(x,r;t)$ in eq 4 can be averaged over the nanopore effective cross section to obtain

$$\frac{\partial \bar{c}(x;t)}{\partial t} = \frac{D}{\pi R_s^2}\int_0^{R_s}\left[\frac{\partial^2 c(x,r;t)}{\partial x^2} + \frac{1}{r}\frac{\partial}{\partial r}\left(r\frac{\partial c(x,r;t)}{\partial r}\right)\right]2\pi r\, dr = D\frac{\partial^2 \bar{c}}{\partial x^2} + \frac{2D}{R_s}\left(\frac{\partial c}{\partial r}\right)_{R_s} \quad (5)$$

At the nanopore surface, the flux density is given by the first-order, irreversible reaction rate[13,14]

$$J_s = -D\left(\frac{\partial c}{\partial r}\right)_{R_s} = kc(x,r = R_s;t) \quad (6)$$

In eqs 4 and 6, $c(x,r;t)$ is the local species concentration, x and r are the axial and radial coordinates, respectively, t is the time, D is the diffusion coefficient, and k is the voltage-dependent reaction rate constant. The concentration in eq 6 corresponds to the solution in contact with the semiconductor surface at $r = R_s$.

$$k(x;t) = k_0 \exp[-\phi_s(x;t)] \approx k_0 \exp\left[V\left[\frac{R - R_s(x;t)}{\lambda} - 1\right]^2\right] \quad (7)$$

with k_0 being the rate constant for $V = 0$. Equation 7 assumes that the electric potential V increases the deposition rate.

Introducing $c(x,r = R_s;t) \approx \bar{c}(x;t)$ in eq 6, eq 5 reads

$$\frac{\partial \bar{c}(x;t)}{\partial t} = D\frac{\partial^2 \bar{c}(x;t)}{\partial x^2} - \frac{2k_0}{R_s(x;t)} \exp\left\{V\left[\frac{R - R_s(x;t)}{\lambda} - 1\right]^2\right\}\bar{c}(x;t) \quad (8)$$

Equation 8 must be solved together with a mass balance equation for the species being deposited. The flux J_s in eq 6 can be related to the increase of the semiconductor layer thickness $R - R_s(x;t)$:

$$J_s = -\frac{1}{\upsilon}\frac{\partial R_s}{\partial t} \quad (9)$$

where υ is the species molar volume. From eqs 6, 7, and 9, we obtain the mass balance equation

$$\frac{\partial R_s(x;t)}{\partial t} = -\upsilon k_0 \exp\left\{V\left[\frac{R - R_s(x;t)}{\lambda} - 1\right]^2\right\}\bar{c}(x;t) \quad (10)$$

Equations 8 and 10 form the basis of the model. They rely on continuum approaches, which are simpler to use than detailed microscopic models and have proved useful for spatial scales greater than 1 nm approximately.[15−19] This system of two coupled partial differential equations in $\bar{c}(x;t)$ and $R_s(x;t)$ must be solved subject to the following initial values

$$\left.\begin{aligned}\bar{c}(x;t=0) &= c_0\\ R_s(x;t=0) &= R\end{aligned}\right\} -L/2 < x < L/2 \quad (11)$$

and boundary conditions

$$\left.\begin{aligned}\bar{c}(x=-L/2;t) &= c_0\\ \bar{c}(x=L/2;t) &= c_0\end{aligned}\right\} 0 < t < \infty \quad (12)$$

Equation 12 is only approximated, since the concentrations at the nanopore mouths may differ from the external solution concentrations because of the decrease in the effective radius of the nanopore as electrodeposition proceeds and the semispherical diffusion zone present at the pore mouths. Both effects should act to decrease this concentration with respect to the bulk value. However, we expect the assumption in eq 12 to give at least the qualitative trends of the problem, since the size of the deposited species is relatively small compared to the nanopore radius (∼10 nm) and the latter is in turn relatively small compared to the nanopore length (∼1000 nm), respectively.

To better understand the limiting cases of eqs 8 and 10, we should identify first the characteristic times of the problem. These are made apparent when we write the equations in dimensionless form as a previous step to solve them numerically. Equation 8 allows us to define the two characteristic time constants (τ_{dif} and τ_{rea}) of the problem, while eq 10 involves the deposition time τ_{dep}:

$$\tau_{dif} = (L^2/D),\ \tau_{rea} = (R/2k_v),\ \tau_{dep} = (R/\upsilon k_v c_0) = (2/\upsilon c_0)\tau_{rea} \quad (13)$$

The first time constant characterizes axial diffusion through the nanopore, which depends on the thickness L. The second time constant is the ratio between the nanopore radius and the potential-dependent reaction rate $k_v = k_0 \exp(V)$. The third time constant concerns radial deposition. The time constant τ_{rea} is much lower than τ_{dep} because $\upsilon c_0 \ll 1$. Note that we include the potential dependence in the reaction rate because we wish to analyze later the effect of the axial dependence on $k(x;t)$ at constant potential V. The relative magnitudes of times τ_{dif} and τ_{rea} in eq 8 dictate the axial concentration profile $\bar{c}(x;t)$.

For fast diffusion ($\tau_{rea} \gg \tau_{dif}$), any decrease of $\bar{c}(x;t)$ in eq 10 should rapidly be smoothed out by axial diffusion and, therefore, $\bar{c}(x;t) \approx c_0$, $-L/2 < x < L/2$. Equation 10 is then trivial and can be readily solved

$$\frac{dR_s(t)}{dt} \approx -\upsilon k_v c_0,\ R_s(t) = R(1 - t/\tau_{dep}) \quad (14)$$

A linear decrease of the nanopore effective radius with time is obtained. Deposition on the nanotube wall proceeds at a constant rate, and the effective radius $R_s(t)$ in Figure 1a shrinks uniformly through the nanopore. The opposite case of fast reaction ($\tau_{rea} \ll \tau_{dif}$) requires analysis of eqs 8 and 10 simultaneously and will be discussed in the next section, although nonuniform deposition could be anticipated in this case. The two limiting cases above can be described in terms of the Damkohler number for the ratio between the reaction to diffusion rates.[13] For extreme values of this number, either kinetics or diffusion controls the process.

Estimation of Parameters. We use the following typical parameters:[1] $\upsilon = 2 \times 10^{-5}$ m^3/mol, $c_0 = 0.1$ mol/m^3, $D = 10^{-9}$ m^2/s, and $R = 2 \times 10^{-8}$ m. Also, we assume that $V = 8$ (0.2 V approximately) and $\lambda = 10^{-7}$ m, a typical value for the depleted layer in semiconductors. The nanopore length is in the range[1] $L = 10^{-6}$−10^{-5} m. Estimation of the reaction rate constant is difficult, however, because it depends on the potential V and the solution properties (e.g., the deposition rate of Te on Au in the absence of Cd is much faster than it is in the presence of Cd[1]). We will consider that $k_v = k_0 \exp(V) = 10^{-7}$−$10^{-5}$ m/s to analyze the different regimes. For $k_v = 10^{-7}$ m/s and $L = 10^{-6}$ m, we obtain $\tau_{dif} = 10^{-3}$ s $\ll \tau_{rea} = 10^{-1}$ s. This is the limiting case where eq 14 applies (fast diffusion). Although the characteristic reaction time τ_{rea} is small, the deposition time $\tau_{dep} \approx 10^6 \tau_{rea}$ is approximately 28 h. The opposite limiting case occurs when $k_v = 10^{-5}$ m/s and $L = 10^{-5}$ m, giving $\tau_{rea} = 10^{-3}$ s $\ll \tau_{dif} = 10^{-1}$ s (fast reaction). The inside diameter decreases now more rapidly at the pore mouths than at the central part of the nanopore, and deposition is no longer uniform. Note finally that τ_{dep}(fast diffusion) $= 10^5$ s $\gg 10^3$ s $= \tau_{dep}$(fast reaction).

3. Results and Discussion

Equations 8 and 10, subject to the initial and boundary conditions of eqs 11 and 12, were solved numerically using the Femlab 3.0 (Comsol AB, 2004) software package. Figures 2−4 show the concentration $\bar{c}(x;t)$ (a) and the nanopore effective radius $R_s(x;t)$ (b) axial profiles for different conditions. The latter profile gives the shape of the inside surface (the deposited semiconductor layer in Figure 1a) through the nanopore. In each figure, the time evolution is given in terms of t_{pro}, defined as the time giving $R_s(L/2;t = t_{pro}) = 0$ at the nanopore mouth. This time can be estimated by integrating eq 10 from $t = 0$ to $t = t_{pro}$.

$$0 = R - \upsilon k_0 c_0 \int_0^{t_{pro}} \exp\left\{V\left[\frac{R - R_s(L/2;t)}{\lambda} - 1\right]^2\right\} dt \quad (15)$$

Equation 15 can be written as

$$\tau_{dep} = [1/\exp(V)] \int_0^{t_{pro}} \exp\left\{V\left[\frac{R - R_s(L/2;t)}{\lambda} - 1\right]^2\right\} dt \quad (16)$$

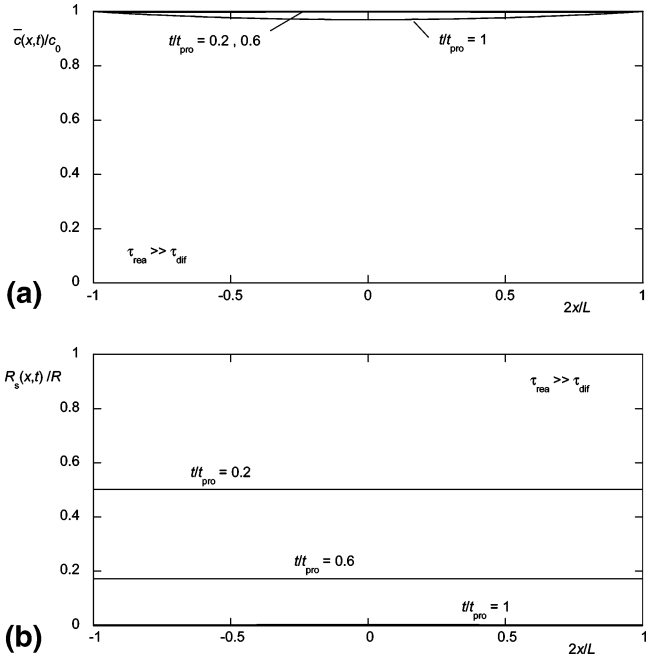

Figure 2. Local concentration $\bar{c}(x;t)$ (a) and nanopore effective radius $R_s(x;t)$ (b) at different times of the deposition process. Time t_{pro} is defined from the condition $R_s(L/2;t = t_{pro}) = 0$ and is proportional to τ_{dep} (see eq 16). We assume $k_v = 10^{-7}$ m/s and $L = 10^{-6}$ m, which give $\tau_{dif} = 10^{-3}$ s $\ll \tau_{rea} = 10^{-1}$ s (fast diffusion; system is reaction controlled).

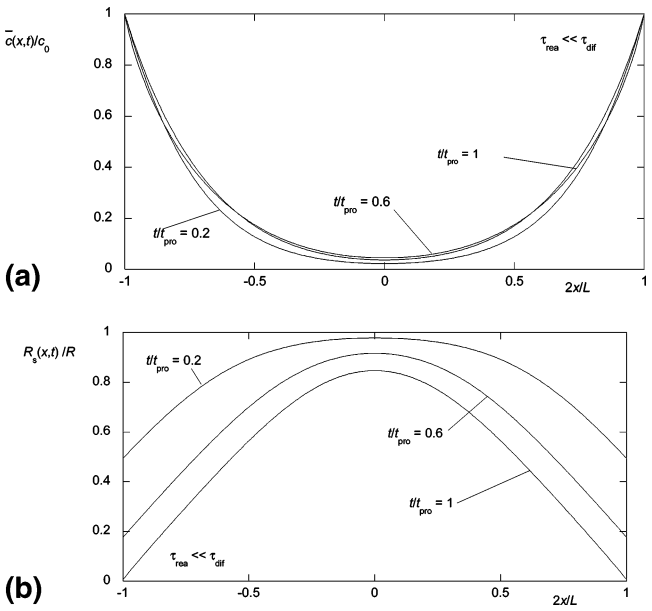

Figure 3. $\bar{c}(x;t)$ (a) and $R_s(x;t)$ (b) for $k_v = 10^{-5}$ m/s and $L = 10^{-5}$ m, which give $\tau_{rea} = 10^{-3}$ s $\ll \tau_{dif} = 10^{-1}$ s (fast reaction; system is diffusion controlled).

which gives times t_{pro} higher than τ_{dep} because $R - R_s < \lambda$ in practical applications ($t_{pro} \approx 6\tau_{dep}$ for the results in Figures 2−4). The parameters $\upsilon = 2 \times 10^{-5}$ m^3/mol, $c_0 = 0.1$ mol/m^3, $D = 10^{-9}$ m^2/s, $R = 2 \times 10^{-8}$ m, $V = 8$ (0.2 V approximately), and $\lambda = 10^{-7}$ m are kept constant in all of the calculations of Figures 2−4.

Figure 2 was obtained with $k_v = 10^{-7}$ m/s and $L = 10^{-6}$ m. Since these values give $\tau_{rea} \gg \tau_{dif}$ (fast diffusion), axial diffusion rapidly compensates for the species depletion following deposition, and this leads to an almost flat concentration profile. Therefore, the effective radius shrinks uniformly through the nanopore. On the other hand, Figure 3 was obtained with $k_v = 10^{-5}$ m/s and $L = 10^{-5}$ m, which give $\tau_{dif} \gg \tau_{rea}$ (fast reaction). Contrary to Figure 2, both concentration and effective radius are not uniform through the nanopore because the reaction is so fast that axial diffusion is no longer able to compensate for the species being deposited. Note the correspondence between the concentration depletion at the nanopore center and the high values of the effective radius there (see eq 10 and Figure 1a). The inside diameters at the pore mouths decrease more rapidly than that at the center of the nanopore. Eventually, the blocking of the nanopore mouths does not allow deposition to proceed further.

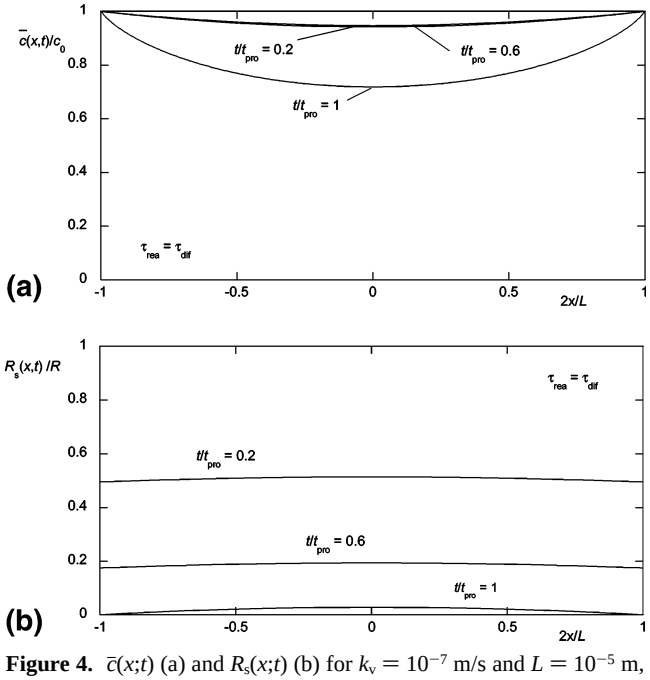

Figure 4. $\bar{c}(x;t)$ (a) and $R_s(x;t)$ (b) for $k_v = 10^{-7}$ m/s and $L = 10^{-5}$ m, which give the intermediate case $\tau_{rea} = \tau_{dif}$ (both diffusion and reaction control the process).

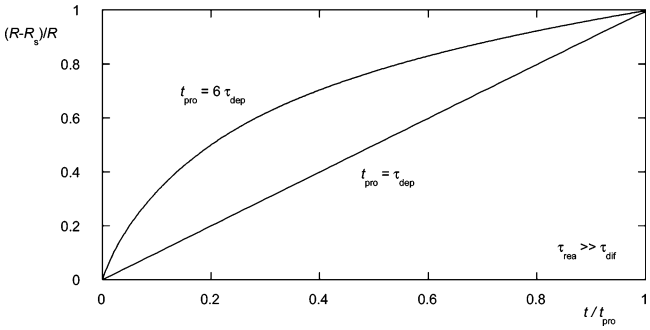

Figure 5. Deposited semiconductor layer thickness at the nanopore mouth normalized to the nanopore radius, $(R - R_s(L/2;t))/R$, as a function of the dimensionless time t/t_{pro} for $\tau_{rea} \gg \tau_{dif}$ (fast diffusion). The top curve corresponds to the results of Figure 2b, while the bottom line is obtained ignoring the axial dependence of the potential in eq 10 ($\phi_s \approx -V$ in eq 7).

Figure 4 was obtained with $k_v = 10^{-7}$ m/s and $L = 10^{-5}$ m, which gives $\tau_{dif} = \tau_{rea}$. Clearly, the results are intermediate between those in Figures 2 and 3. Note that, contrary to the case of Figure 2b, the deposition could not be completed under the conditions of Figures 3b (fast reaction) and 4b (intermediate case) because of the blocking of both nanopore mouths leaving the central region devoid of semiconductor.

Figure 5 shows the deposited semiconductor layer thickness at the nanopore mouth normalized to the nanopore radius, $(R - R_s(L/2;t))/R$, as a function of the dimensionless time t/t_{pro} for $\tau_{rea} \gg \tau_{dif}$ (fast diffusion). The top curve corresponds to the

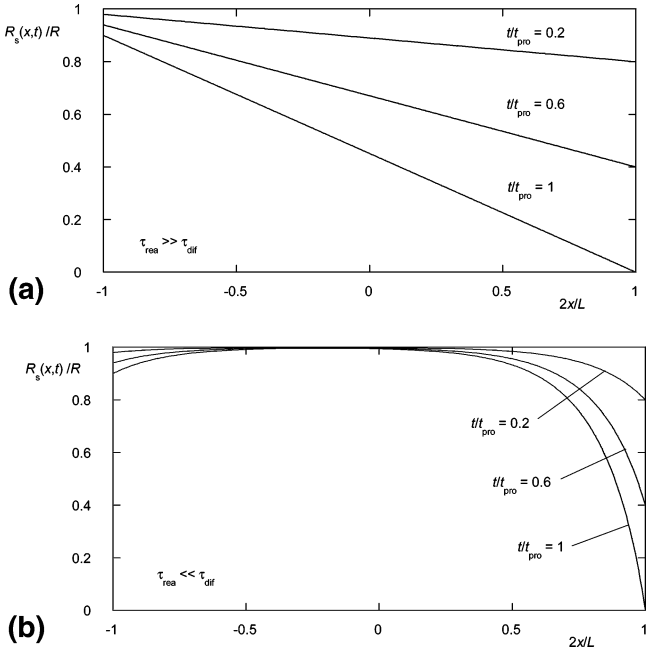

Figure 6. $R_s(x;t)$ for the fast diffusion case of Figure 2b (a) and the fast reaction case of Figure 4b (b). The boundary and initial conditions are now $\bar{c}(-L/2;t) = c_0 \ll 10c_0 = \bar{c}(L/2;t)$ and $\bar{c}(x;0) = c_0[1 + 9(x/L + 1/2)]$, respectively, which correspond to a concentration gradient through the nanopore. In this case, $t_{pro} \approx 0.1\tau_{dep}$.

results of Figure 2b, while the bottom line corresponds to a limiting situation where the axial dependence of the potential in eq 10 is ignored ($\phi_s \approx -V$ in eq 7). Note the different times t_{pro} (see eq 16) and deposition rates (see eq 10) obtained when the effect of the axial potential is introduced in the reaction rate constant, which is the case of the top curve. Preliminary experimental data on flat surfaces (unpublished results) show the trends of the top curve. The decrease of the process characteristic time from $t_{pro} \approx 6\tau_{dep}$ (top curve) to $t_{pro} \approx \tau_{dep}$ (bottom line) is caused by the higher effective rate constant of the latter case (note that $k(x;t) \leq k_v$ in eq 7).

Since axially uniform nanocables are required for most applications, we have considered so far the effects of the reaction and axial diffusion rates on the deposition. However, for nanoporous membranes, other (e.g., conical[2]) geometries may be desirable. This is the case of single nanoparticle detection using membranes with nanopores.[2,19] Therefore, we address finally the conditions where asymmetric nanopores, as opposed to symmetric nanocables, could be experimentally realized. Figure 6 shows $R_s(x;t)$ for $\tau_{rea} \gg \tau_{dif}$ (a), the fast diffusion case of Figure 2b, and $\tau_{rea} \ll \tau_{dif}$ (b), the fast reaction case of Figure 3b, with $\phi_s \approx -V$ in eq 7. However, the boundary and initial conditions are now $\bar{c}(-L/2;t) = c_0 \ll 10c_0 = \bar{c}(L/2;t)$ and $\bar{c}(x;0) = c_0[1 + 9(x/L + 1/2)]$, respectively, which are different from those in Figures 2−5 and correspond to a concentration gradient through the nanopore. These conditions give $t_{pro} \approx 0.1\tau_{dep} < \tau_{dep}$, contrary to the previous cases, because now the right solution concentration $10c_0$ substitutes for c_0 in eq 15 (we still define τ_{dep} in terms of the left solution concentration c_0; see eq 13).

We consider now the time evolution of the nanopore asymmetric characteristics. Figure 7 shows the left, $R_s(-L/2;t)$, and right, $R_s(L/2;t)$, inside radii normalized to the original radius R for the conical nanopore of Figure 6a as a function of the dimensionless time t/t_{pro}. It is apparent from the above figures that highly asymmetric nanopores could be obtained by allowing the reaction to proceed only for a reduced time $t < t_{pro}$, avoiding

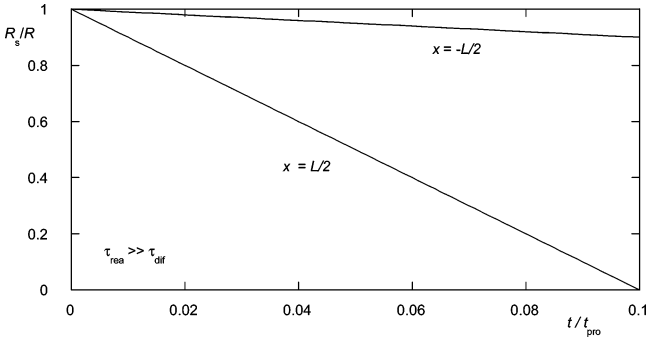

Figure 7. Left ($R_s(-L/2;t)$) and right ($R_s(L/2;t)$) inside radii normalized to the original nanopore radius R for the conical nanopore of Figure 6a as a function of the dimensionless time t/t_{pro}.

thus the blocking of the pore mouths (see Figure 1a). In particular, Figure 6a shows that conical nanopores result for the case of fast diffusion and Figure 7 gives the maximum and minimum nanopore radii as a function of time. It is clear that use of different axial concentration gradients would allow further control of the inside diameters at the left and right nanopore mouths, respectively. Figure 6b corresponds to the opposite limiting case of fast reaction, suggesting that different time regimes could give a variety of externally controlled asymmetric structures. These effects could be even more marked for lower values of the original nanopore radius R.

4. Conclusion

In conclusion, the model gives predictions concerning the nanocable synthesis as a function of the deposited species concentration, the nanopore dimensions, and the voltage-dependent reaction rate (which changes with the axial position and time). Moreover, in those cases where an asymmetric deposition should be desirable, the experimental conditions making it possible are given and the resulting profile for the inside diameter through the nanopore is predicted. Extensions of the model could also be useful for other multiscale (nanometers for the nanopore radius and micrometers for the thickness) nanosystems where diffusion and reaction limitations can be present simultaneously as well as for the analysis of multilayer nanocable fabrication.

Acknowledgment. Financial support from the CICYT, Ministerio de Ciencia y Tecnología (Project No. MAT2005-01441), and the University of Valencia Visiting Professorship program (K.L.) is acknowledged. We are grateful to Prof. José A. Manzanares for helpful discussions.

References and Notes

(1) Ku, J.-R.; Vidu, R.; Talroze, R.; Stroeve, P. *J. Am. Chem. Soc.* **2004**, *126*, 15022−3.

(2) Mara, A.; Siwy, Z.; Trautmann, C.; Wan, J.; and Kamme, F. *Nano Lett.* **2004**, *4*, 497−501.

(3) Léger, C.; Elezgaray, J.; Argoul, F. *Phys. Rev. E* **1998**, *58*, 7700−9.

(4) Sochnikov, V. S.; Efrima, S. *J. Phys. Chem. B* **2002**, *106*, 11993−9.

(5) Valizadeh, S.; George, J. M.; Leisner, P.; Hultman, L. *Electrochim. Acta* **2001**, *47*, 865−74.

(6) Varazo, K.; Lay, M. D.; Sorenson, T. A.; Stickney, J. L. *J. Electroanal. Chem.* **2002**, *522*, 104−14.

(7) Sorenson, T. A.; Varazo, K.; Suggs, D. W.; Stickney, J. L. *Surf. Sci.* **2001**, *470*, 197−214.

(8) Sima, M.; Enculescu, I.; Trautmann, C.; Neumann, R. *J. Optoelectron. Adv. Mater.* **2004**, *6*, 121−5.

(9) Solymar, L.; Walsh, D. *Electrical properties of materials*; Oxford University Press: Oxford, U.K., 1998.

(10) Wang, S. *Fundamentals of semiconductor theory and device physics*; Prentice Hall: Englewood Cliffs, NJ, 1989.

(11) Van Zeghbroeck, B. *Principles of Semiconductor Devices*; University of Colorado, Boulder, 2004 (http://ece-www.colorado.edu/~bart/book/).

(12) Murphy, W. D.; Manzanares, J. A.; Mafé, S.; Reiss, H. *J. Phys. Chem.* **1992**, *96*, 9983−91.

(13) Cussler, E. L. *Diffusion*: *mass transfer in fluid systems*; Cambridge University Press: Cambridge, U.K., 1997.

(14) Crank, J. *The mathematics of diffusion*; Oxford University Press: Oxford, U.K., 1999.

(15) Ramirez, P.; Mafé, S.; Alcaraz, A.; Cervera, J. *J. Phys. Chem. B* **2003**, *107*, 13178−87.

(16) Ramírez, P.; Mafé, S.; Aguilella, V. M.; Alcaraz, A. *Phys. Rev. E* **2003**, *68*, 011910−6.

(17) Fulinski, A.; Rosinska, A.; Siwy, Z. *Europhys. Lett*. **2004**, *67*, 683−9.

(18) Harrell C. C.; Lee, S. B.; Martin, C. R. *Anal. Chem.* **2003**, *75*, 6861−7.

(19) Lee, S.; Zhang, Y.; White, H. S.; Harrell, C. C.; Martin, C. R. *Anal. Chem.* **2004**, *76*, 6108−15.